# FAST ESTIMATION OF CRS PARAMETERS USING LOCAL SLOPES IN INHOMOGENEOUS MEDIA

*L.T. Santos, J. Schleicher, J.C. Costa, and A. Novais*

**email:** *lucio@ime.unicamp.br*

**keywords:** *Local slopes, CRS, parameter estimation*

**ABSTRACT**

*Conventional techniques to estimate the traveltime parameters of the common-reflection-surface (CRS) stack are tedious, time-consuming, and expensive processes based on local coherence analyses along a large number of trial surfaces. Recently, we demonstrated that the 2D CRS method can be sped up by several orders of magnitude by an application of modern local-slope-extraction techniques. As shown through numerical examples for homogeneous media, the complete set of CRS parameters can be extracted from seismic data. The necessary information about the CRS parameters is contained in the slopes of the common-midpoint section at the central point and one or several common-offset sections in its vicinity. In this work, we apply the technique to more realistic velocity models and compare the results to a simplified implementation of a conventional CRS procedure. Our numerical examples demonstrate that the technique lead to meaningful values for the CRS parameters for inhomogeneous media.*

## INTRODUCTION

Present-day techniques to estimate the traveltime parameters of the common-reflection-surface (CRS) stack rely on the analysis of the local coherences along a large number of trial surfaces for a set of possible parameter combinations. Even in 2D, this analysis is a tedious and time-consuming process (see, e.g., Jäger et al., 2001; Hertweck et al., 2007). Fast alternatives have been proposed recently (Santos et al., 2009; Santos and Schleicher, 2010; Kazinnik and Burnett, 2010).

However, there is another way of extracting traveltime attributes, particularly local slopes, which has received strong attention in the recent past (Fomel, 2002; Schleicher et al., 2009). The reason is that local slopes of seismic events are useful in a variety of seismic imaging processes. Perhaps, the most visible ones are those connected with seismic tomography, in which not only traveltimes but also slownesses of events and possible other time-domain attributes are used to build a velocity model. Most prominent examples are slope tomography (Sword, 1987; Biondi, 1990), stereotomography (Billette and Lambaré, 1998; Billette et al., 2003) and normal-incidence-point (NIP) wave tomography (Duveneck, 2004).

The conventional procedure to extract the local event slope relies on local slant stacks (Ottolini, 1983a). In this method, a local coherence analysis is carried out at each point in the seismic section along short straight-line elements in all possible directions. The direction with the highest coherence defines the slope value at that point.

However, the local-slant-stack approach to local-slope extraction has a number of drawbacks. First of all, the method has a high computational cost. Since the space of local slopes must be closely sampled, there is a high number of coherence analyses to be carried out. The second drawback lies in the method's sensitivity to the aperture of the local slant stacks. An adequate aperture is problem dependent and thus hard to know in advance. Finally, as demonstrated by Schleicher et al. (2009), the extracted slopes are not always reliable, but can be biased towards too high dips.

As discussed by Fomel (2002), there exist more modern and faster techniques to directly extract local slopes from prestack data without the need for local coherence analyses. His technique was later improved by Fomel (2007a,b) using shaping regularization for optimal smoothness control. Schleicher et al. (2009) compared a set of alternative, fast and reliable ways to extract local slopes.

It is known that the normal-moveout (NMO) velocity is directly related to the local slope of a seismic event in a common-midpoint (CMP) section (Ottolini, 1983b). Therefore, the natural question arises whether the other CRS parameters can also be related to local slopes, so that the complete set of CRS parameters can be determined using these kinds of techniques. In this paper, we show how the CRS parameters relate to local slopes and use this information in order to speed up their extraction. Of course, this relationship is most straightforward for the emergence angle of the normal ray, $\beta$, since this parameter directly represents a local slope. The slope extraction techniques can be extended to allow for the extraction of the complete set of CRS parameters.

In previous works (Santos et al., 2008; Santos and Schleicher, 2009) we discussed two procedures for the extraction of CRS parameters from local slopes and showed constant-velocity examples as a proof of concept. In this paper, we apply the technique to more realistic examples and compare the results to a simplified implementation of a conventional CRS procedure. Our numerical examples demonstrate that the technique lead to meaningful values for the CRS parameters for laterally varying velocity models.

## CRS TRAVELTIMES AND LOCAL SLOPES

The common-reflection-surface (CRS) stack was first presented in two talks at the 1998 EAGE conference by Hubral et al. (1998a) and by Müller (1998). Like Multifocusing (see, e.g., Landa et al., 1999), it was motivated by the Common-Reflection-Element method (Gelchinsky, 1988, 1989) and is based on the same ideas and principles as the conventional common-midpoint (CMP) stack. The basic difference is that a CRS stack uses far more traces than those present in a CMP gather. For each stacking trace location (the central point), the CRS method considers a supergather of source-receiver pairs, arbitrarily located with respect to the central point. In other words, the CRS stack uses not only the CMP gather at the central point, but also neighbouring gathers. In this way, the CMP stacking line turns into a CRS stacking surface.

Of course, in order to make use of the additional data dimension in the off-CMP (or relative midpoint coordinate) direction, we need additional traveltime parameters to describe the stacking surface. In 2D, the general traveltime function in the midpoint-offset domain depends now on three independent parameters. In addition to the normal-moveout (NMO) velocity, there is a parameter related to the local slope of the traveltime curve at zero-offset and one related to the local curvature at zero-offset, which depends on the reflector curvature. In the CRS stack, these three parameters are determined for each central point and all values of the zero-offset traveltime. The procedure is performed automatically, with no a priori selection of traveltime samples.

In previous works, the three CRS traveltime parameters have been related to physical parameters in the model space (Jäger et al., 2001) or in the data space (Hertweck et al., 2007). In the most simple mathematical parametrization in two dimensions, the (generalized) hyperbolic moveout, i.e., the CRS stacking surface, can be represented as

$$T_{CRS}(x,h) = \sqrt{[T_0 + A\,(x-x_0)]^2 + B\,(x-x_0)^2 + C\,h^2}, \tag{1}$$

where $x$ and $h$ denote the midpoint and half-offset coordinates of the source and receiver pair, $x_0$ is the midpoint coordinate of the central point, and $T_0 = T_{CRS}(x_0, 0)$ is the zero-offset (ZO) traveltime at the central point. As shown in Hubral et al. (1998b), the parameters $A$, $B$ and $C$ are related to physical model-space quantities $\beta$, $K_N$ and $K_{NIP}$, often also referred to as the CRS parameters or attributes, by the relationships

$$A = \frac{2\sin\beta}{v_0}, \quad B = \frac{2T_0\cos^2\beta}{v_0}K_N, \quad \text{and} \quad C = \frac{2T_0\cos^2\beta}{v_0}K_{NIP}, \tag{2}$$

where $v_0$ denotes the near-surface medium velocity at the central point. The physical meaning of these parameters are: Angle $\beta$ is the emergence angle of the ZO ray with respect to the surface normal, and $K_N$ and $K_{NIP}$ are the curvatures of the normal (N) and normal-incidence-point (NIP) waves, respectively (see

Hubral, 1983). We observe from equations (1) and (2) that the original CRS parameters $\beta$, $K_N$, and $K_{NIP}$ can be calculated for a given $T_0$ once all three parameters $A$, $B$, and $C$, as well as the near-surface velocity $v_0$, are known. However, for the detection of the parameters $A$, $B$, and $C$, no knowledge of the near-surface velocity $v_0$ is required.

As we will show below, the CRS parameters can be expressed entirely as a function of local slopes of the reflection traveltime surfaces in the common-midpoint (CMP) and common-offset (CO) sections. In the following discussion, we will use capital letters $T$ when talking about theoretical traveltime functions or values and lowercase letters $t$ when talking about time coordinates in seismic sections. Correspondingly, we use lowercase letters, $a$, $b$, and $c$ for the CRS parameters when referring to preliminary local estimates from local slopes in the data sections and reserve the uppercase letters for the final average parameters already attributed to parameter maps the coordinates of which are the central point $x_0$ and zero-offset traveltime $t_0$.

### Common-midpoint traveltime

In the situation of a single (horizontal) seismic line and within a given CMP gather, namely source-receivers pairs that are symmetrically located around a fixed central point $x_0$, the general CRS traveltime formula (1) reduces to the well-known NMO traveltime function,

$$T_{CMP}(h) = T_{CRS}(x_0, h) = \sqrt{T_0^2 + C\ h^2}. \tag{3}$$

In the above equation, $T_{CMP}$ is the traveltime from the source to the reflector and back to the receiver, $h$ is the source-receiver half-offset, and $T_0 = T_{CMP}(0)$ is interpreted, as before, as the ZO traveltime at $x_0$, i.e., the traveltime along the normal ray that emerges at the central point of the CMP gather.

Under the usual assumption of a horizontally stratified (or small-dip) media, the ray parameter for the reflection ray in the CMP gather with fixed central point (midpoint) $x_0$, can be approximated by the traveltime slope (see, e.g., Castagna and Backus, 1993). The derivative of equation (3) with respect to source-receiver offset $2h$ yields

$$p = \frac{1}{2}\frac{d}{dh}T_{CMP} = \frac{C\ h}{2\ T_{CMP}}. \tag{4}$$

Thus, if we know the local slope $p = p(h,t)$ at a point $(h,t)$ in a CMP gather, we can use equations (3) and (4) to eliminate $C$ from the moveout equation (3). This provides us with the NMO coordinate map (Ottolini, 1983b)

$$t_0 = \sqrt{t^2 - 2\ h\ t\ p(h,t)}\ , \tag{5}$$

which describes the relationship between the coordinates $(h,t)$ in a CMP section and the corresponding zero-offset time $t_0$ at $x_0$. Equation (5) can be immediately used for an automatic NMO correction (Wolf et al., 2004; Fomel, 2007b; Schleicher et al., 2009), since it tells us how to move a pixel of information from coordinates $(h,t)$ in the CMP section to $(h,t_0)$ in the NMO corrected section.

On the other hand, equation (4) provides us with the first relationship between a curvature parameter and a local slope. Rewriting equation (4), we see that an estimate of parameter $C$ at half-offset $h$ and time $t$ is given by

$$c(h,t) = \frac{2\ t\ p(h,t)}{h}. \tag{6}$$

From equation (6), we infer the procedure that achieves the determination of parameter $C$. All that needs to be done is to correct the extracted local slope $p$ at a position $(h,t)$ in the CMP section with the factor $2t/h$ and then to transfer the obtained value of $c$ to the $C$-parameter section at $(x_0,t_0)$ using equation (5). This can be done fully automatically. Since there is redundant information from all half-offsets, the final $C(x_0,t_0)$ can be calculated by averaging over all $c(h,t)$ that correspond to the same $(x_0,t_0)$. In our numerical examples, this averaging uses the coherence measure associated with the extracted $p$ at $(h,t)$ as a weight function. The determination of the coherence measure associated with $p$ is explained below.

### Common-offset traveltime

The remaining two CRS parameters, $A$ and $B$ can be determined from a CO gather in the vicinity of $x_0$. This is advantageous over the conventional detection in the ZO gather, because the latter is only available after stack and its quality already depends on $C$, while CO gathers are available in the original data, thus permitting a determination of $A$ and $B$ that is completely independent of possible errors already committed in the determination of $C$.

For the case of a CO gather with a fixed half-offset $h = h_0$, formula (1) reduces to

$$T_{CO}(x) = T_{CRS}(x, h_0) = \sqrt{T_{CMP}(h_0)^2 + 2\,A\,T_0\,(x - x_0) + D\,(x - x_0)^2}, \tag{7}$$

where the new parameter $D$ is given by $D = A^2 + B$, and $T_{CMP}$ is the traveltime for the offset ray with midpoint at $x_0$. It is given in terms of the ZO traveltime $T_0$ by equation (3) with $h = h_0$.

From traveltime formula (7), we see that the local slope $q$ at a point $(x, t = T_{CO}(x))$ in the CO gather is given by

$$q = \frac{d}{dx} T_{CO} = \frac{A\,T_0 + D\,(x - x_0)}{T_{CO}}. \tag{8}$$

For the determination of $A$ and $B$, we assume that the local slope $q = q(x, t)$ is known at all positions $(x, t)$ in the CO gather in a sufficiently large vicinity of $x_0$, and that it is sufficiently well approximated by

$$q(x, t) = \frac{A\,T_0 + D\,(x - x_0)}{t}, \tag{9}$$

which is exactly true at $t = T_{CO}(x)$.

Using $x = x_0$ in the above formula, we arrive at the following estimates for $A$ and $B$,

$$a(x_0, t) = \frac{q(x_0, t)\,t}{t_0}, \quad \text{and} \quad b(x, t) = \frac{t\,[q(x, t) - q(x_0, t)]}{x - x_0} - a(x_0, t)^2,\ x \neq x_0. \tag{10}$$

Unfortunately, estimate $b$ is still associated with a point $(x, t)$ in the CO section instead of a point $(x_0, t_0)$ in the final parameter section with zero-offset coordinates. Moreover, while $x_0$ is known as the coordinate of the present central point, the zero-offset traveltime coordinate $t_0$ that corresponds to the common-offset traveltime coordinate $t$ is still unknown and must be determined. For this purpose substituting the above estimates of $a$ and $b$ in equation (7), and solving for the CMP traveltime, we obtain the coordinate map

$$t_{CMP} = \sqrt{t^2 - t\,(x - x_0)\,[q(x, t) + q(x_0, t)]}, \tag{11}$$

between the CO and CMP sections. Map (11) can be executed once $q$ has been detected at every point $(x, t)$ in the CO section. As a last step, the time coordinate $t_{CMP}$ must be related to its associated ZO traveltime coordinate $t_0$. This can be done using formula (5), i.e.,

$$t_0 = \sqrt{t_{CMP}^2 - 2\,h_0\,t_{CMP}\,p(h_0, t_{CMP})}, \tag{12}$$

where $p(h_0, t_{CMP})$ is the local slope at the coordinates $h = h_0$ and $t = t_{CMP}$ in the CMP section at $x_0$, extracted during the determination of $C$.

The final sections for $A$ and $B$ as a function of $x_0$ and $t_0$ are then constructed. Note that all these estimates $a(x_0, t)$ and $b(x, t)$ for all points $(x, t)$ in the CO section pertain to one and the same chosen central point $x_0$. However, they still need to be transfered to the point $(x_0, t_0)$ in the parameter sections, where $t_0$ is given by equation (12). The mapping procedure is illustrated in Figure 1. The transfer of $a(x_0, t)$ to the point $(x_0, t_0)$ in the final $A$ parameter section is straightforward using the traveltime coordinate map composed by equations (12) and 11. The transfer of $b(x, t)$ to the point $(x_0, t_0)$ in the $B$ parameter section is done analogous as for the case of the $C$ parameter section. Many estimates of $b(x, t)$ will be attributed to the same ZO time $t_0$. In our numerical experiments, we used estimates from up to 500 m distance from the central point. Thus, $B(x_0, t_0)$ need to be calculated by averaging over all $b(x, t)$, respectively, that correspond to the same $(x_0, t_0)$. Again, our numerical implementation of this averaging uses coherence-measure weights.

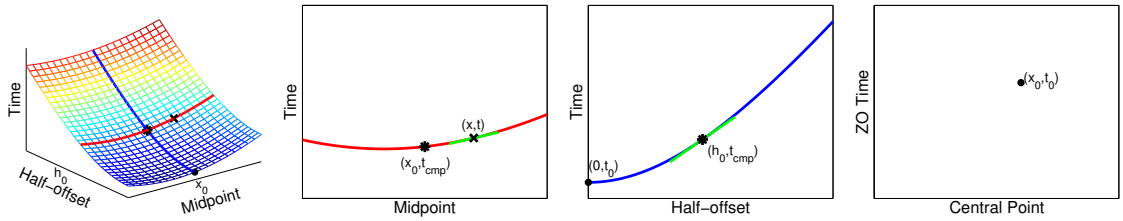


**Figure 1:** Mapping of the parameter estimates $a$, $b$, and $c$ to their position at $(x_0, t_0)$ in the final $A$, $B$, and $C$ parameter sections. (a) 3D view of the CRS traveltime surface. Also shown are the CO traveltime $T_{CO}(x)$ (red line) and CMP traveltime $T_{CMP}(h)$ (blue line), as well as points $(x, h, t)$ (cross), $(x_0, h, t_{CMP})$ (asterisk), and $(x_0, 0, t_0)$ (dot). (b) CO section with half-offset $h_0$ around $x_0$. Slope $q$ (green line) of traveltime curve $T_{CO}(x)$ (red line) at $(x, t)$ (cross) is detected and used to determine $t_{CMP}$ at $x_0$ (asterisk) from equation (11). (c) CMP section at $x_0$. Slope $p$ (green line) of traveltime function $T_{CMP}(h)$ (blue line) at $(h, t_{CMP})$ (asterisk) is detected and used to determine the zero-offset traveltime $t_0$ at $x_0$ (dot) from equation (12). (d) The final parameter value is obtained as an average of all estimates that are attributed to the same point $(x_0, t_0)$ (dot) in the parameter section.

For the extraction of $A$ and $B$, further data redundancy is avaliable. The mapping procedure described here for a single constant half-offset $h_0$ can be applied for different CO sections around the central point $x_0$. The final values of $A$ and $B$ can then be obtained by averaging over all values that are attributed to the same point $(x_0, t_0)$ from all different CO sections used in the process. However, since the traveltime approximations are valid in the vicinity of the normal ray, too far offsets should be avoided.

## EXTRACTING THE LOCAL SLOPES

The extraction of local slopes is done by so-called plane-wave destructors. The differential equation that describes a local plane-wave event in a seismic section is given by (Claerbout, 1992)

$$\psi_y(y,t) + s\ \psi_t(y,t) = 0, \tag{13}$$

where $\psi(y,t)$ is the wavefield, $t$ is the time coordinate, and $y$ is the horizontal coordinate, i.e., offset ($2h$) in the case of a CMP section or midpoint ($x$) in the case of a CO section. Also, $\psi_y$ and $\psi_t$ denote the derivatives of $\psi$ with respect to $y$ and $t$, respectively. Quantity $s$ represents the local slope (i.e., $p$ or $q$ in a CMP or CO section), which may depend on $y$ and even on $t$, i.e., generally, $s = s(y,t)$.

To extract the slopes, we use basically the plane-wave destructor technique presented in Claerbout (1992), Fomel (2002), and Schleicher et al. (2009) with the modification reported in Santos et al. (2009), where a few small alterations in the implementation were done to make the process more stable.

## SYNTHETIC EXAMPLES

We tested our extraction techniques with synthetic data from models with different complexity. The first model is a very simple one consisting of homogeneous layers. For a more realistic test, we extracted the CRS parameters from the Marmousoft data and compared the results to those from a fast implementation of the conventional CRS method.

### Simple data

The model for the first numerical experiments consists of a stratified medium with five homogeneous layers between two homogeneous half-spaces (see Figure 2). The velocity for the shallowest reflector was 4.0 km/s, increasing by 0.2 km/s for each layer to 5.0 km/s for the deepest one. We simulated CMP sections with 100 half-offsets ranging from $-1$ km to 1 km, for 41 central-points between 1 km and 9 km, and one CO section with half-offset 500 m containing 361 midpoints between 500 m and 9.5 km. In all simulations

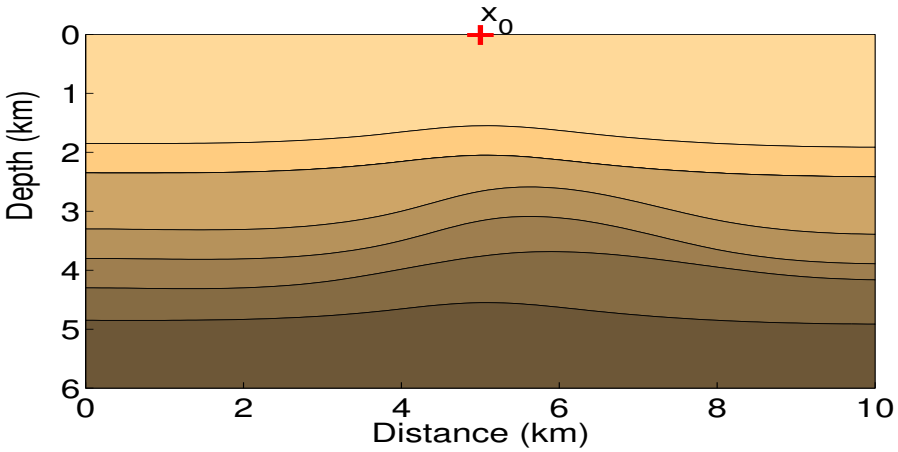


**Figure 2:** Synthetic model for the experiments.

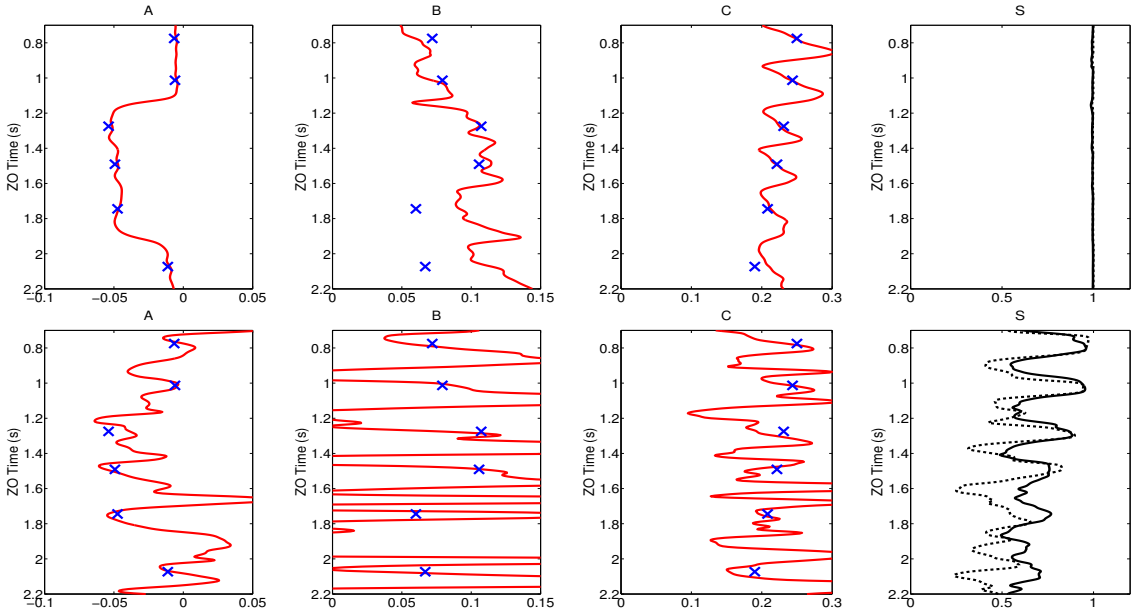


**Figure 3:** CRS parameters ($A$, $B$, $C$) and semblances ($S$). The exact are the blue crosses and the estimated ones are the red lines. Top: Noise-free data; bottom: Noisy data.

the time sampling was 4 ms. We tested the performance of the parameter extraction on data with and without random white noise. For the noisy-data example, the signal-to-noise ratio was 3.

We start by showing the results at a single central point, $x_0 = 5$ km. This central point is also shown in Figure 2. The values of the extracted CRS parameters $A$, $B$ and $C$ at the chosen point $x_0$ (only one trace) for noise-free data are shown in the top of Figure 3. The extracted values (red lines) are depicted together with the respective exact values (blue crosses). Of course, true values are only available at the reflection events while the extraction procedure yields values at all times. This figure also shows the values of the accumulated semblances ($S$) for $p$ and $q$. These are the mean values of the semblances of all values of the parameters $A$, $B$ and $C$ that contributed to the final values. As usual for noise-free data, the semblance is very high everywhere.

The corresponding results using noisy data are shown in the bottom of Figure 3. As we can see in these figures, the presence of noise does not alter the above observations. The results are still highly satisfactory. Parameters $A$ and $C$ have lost almost no quality in comparison to the noise-free situation. It is to be noted

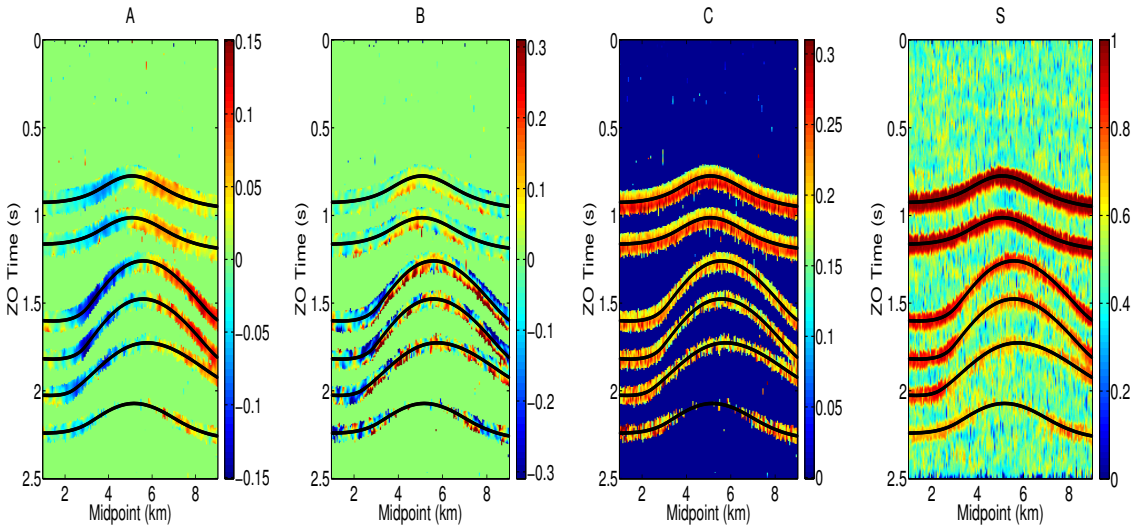


**Figure 4:** CRS parameters and semblance sections for data with 30% noise. Parameter values at points where semblance is below 0.7 were muted.

that for the noisy data, the accumulated semblance $S$ exhibits significant peaks at the actual reflection times, thus carrying useful information on where the extracted parameter values are actually reliable. This behavior is the same for both techniques. These numerical experiments demonstrate that the estimation of CRS parameters from local slopes is sufficiently stable to permit their automatic extraction, even for noisy data. We stress again that this extraction technique is orders of magnitude faster than the conventional CRS method that uses local coherence analyses.

To demonstrate the quality of the proposed parameter extraction, Figure 4 shows the parameter panels resulting from applied the described technique to the noisy data, for all 41 central-points. The panels as masked with the semblance section, muting all parameter values at points where the semblance value is below 0.5. Also shown in Figure 4 are the positions of the reflection events in the zero-offset section (black lines). All three parameter panels exhibit the expected behavior. The $A$ section contain negative (blue) values where the events dip to the left and positive (red) values where the events dip to the right. The $B$ section exhibits the corresponding behaviour for positive and negative curvatures. Finally, the $C$ section exhibits decreasing values from top to bottom, in correspondence with the increasing rms velocity in the model. For a more quantitative analysis of the extracted parameter values, we plot in Figure 5 the values of $A$, $B$ and $C$ along the reflection event of the 3rd reflector.

### Marmousoft data

For a better assessment of the quality of the extracted parameters in a more realistic situation, we test the performance of the fast CRS parameter extraction on the Marmousoft data (Billette et al., 2003) and compare its results with those from a simplified implementation (fast global parameter optimization without careful treatment of local minima, no conflicting dip handling, no smoothing) of the conventional CRS procedure. The fast parameter extraction using local slopes took about half an hour using a simple Matlab implementation, while the simplified CRS procedure still lasted almost one hour in a Fortran 90 implementation. A full CRS treatment would take about one to two orders of magnitude more computer time.

Figures 6 to 11 compare the results of the two procedures. In Figure 6, we see the extracted values of parameter $A$ from local slopes (top) and from CRS (bottom). While the CRS result presents some more detail, the overall results are comparable. Roughly, the slope-derived section (top) looks like a smoothed version of the CRS-derived section (bottom). Figure 7 shows the extracted values of parameter $B$ from local slopes (top) and from CRS (bottom). As for parameter $A$, the CRS result presents some more detail, but the overall results exhibit the same general behavior. Note, however, that the range of $B$ values from the CRS procedure is somewhat larger than from the slopes. Figure 8 shows the extracted values of parameter

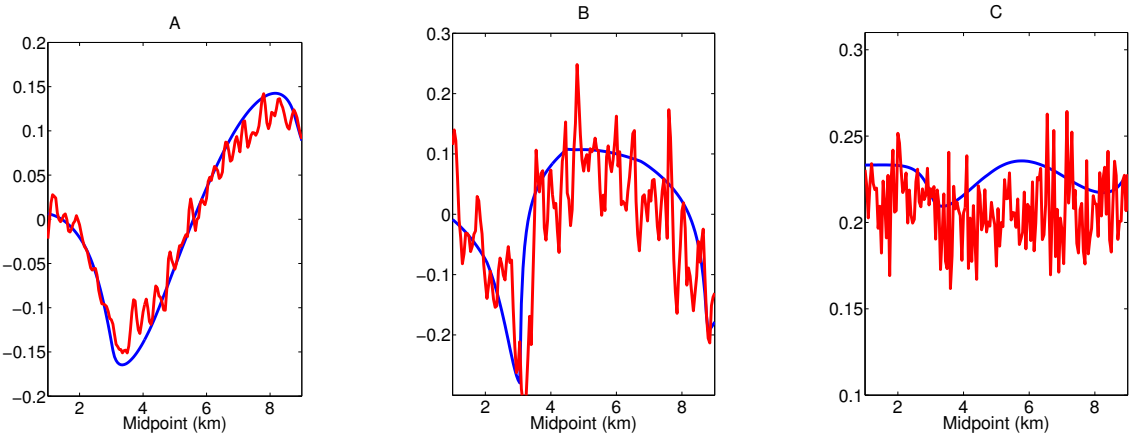


**Figure 5:** Parameters $A$, $B$ and $C$ along the ZO reflection event for the 3rd reflector and data with 30% noise: true values (blue line) are compared to values extracted (red line).

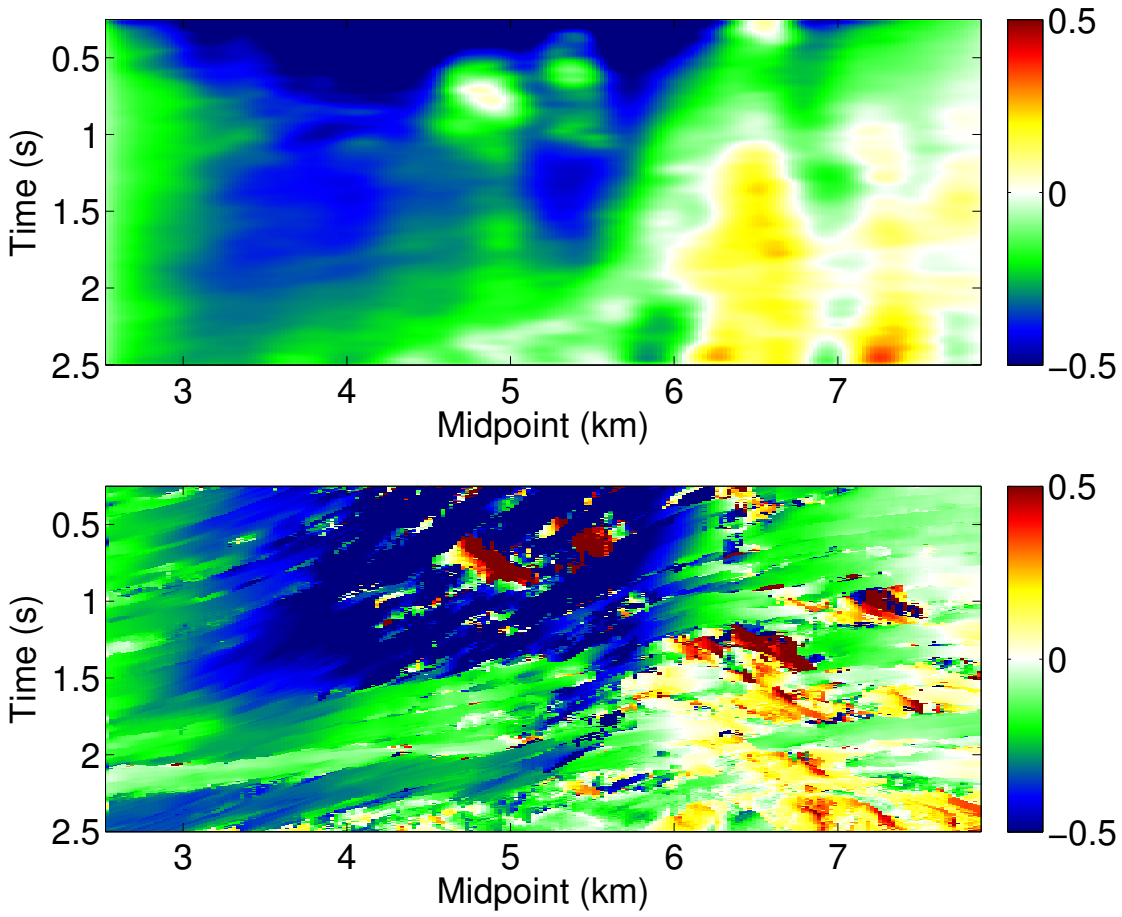


**Figure 6:** Values of CRS parameter $A$ as extracted using local slopes (top) and a simplified CRS procedure (bottom).

$C$ from local slopes (top) and from CRS (bottom). The fact that $C$ is the most stable parameter is reflected in the very strong resemblance of the two figures. Again, we notice some more detail in the CRS result.

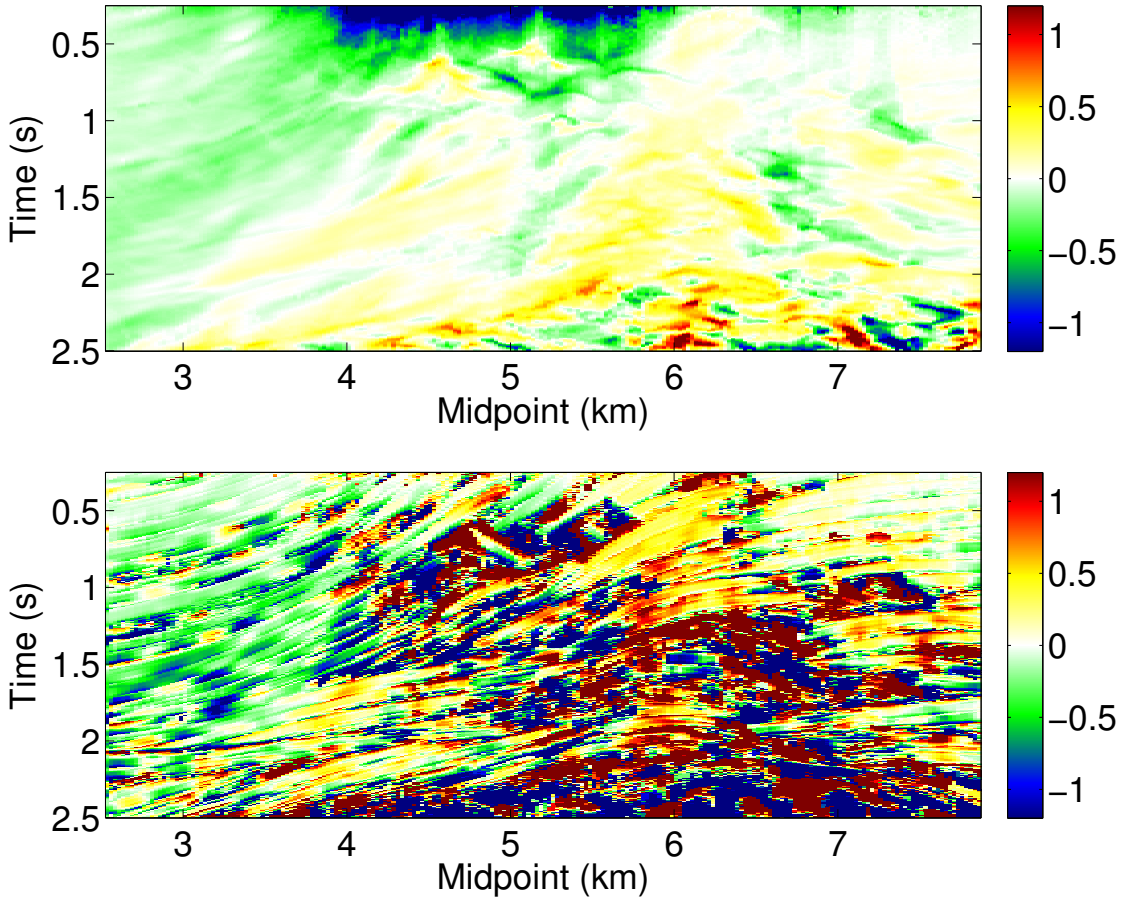


**Figure 7:** Values of CRS parameter $B$ as extracted using local slopes (top) and a simplified CRS procedure (bottom).

Generally, we can think of the slope-extracted CRS parameters as a little smoother than those from conventional CRS. Figure 9 depicts the semblance sections using the extracted values of the CRS parameters $A$, $B$, and $C$ from local slopes (top) and from CRS (bottom). Both semblance sections exhibit rather high semblance values, indicating the high quality of the extracted traveltime surfaces. The CRS semblance section is overall a little darker than the slope semblance section, indicating that the conventionally extracted CRS parameters are doing a slightly better job of approximating the true reflection traveltimes.

Figure 10 depicts the stacked sections using the extracted values of the CRS parameters $A$, $B$, and $C$ from local slopes (top) and from CRS (bottom). While the CRS stacked section is still slightly superior to the one obtained using the parameters derived from local slopes, the quality of the latter is still satisfactory. For comparison, the nearest-offset section (with a source-receiver offset of 100 m) is depicted in Figure 11. This section and both stacked sections in Figure 10 agree reasonably well, demonstrating the good quality of the stack and the underlying CRS parameters.

## CONCLUSIONS

CRS parameter extraction by local coherence analysis has a number of drawbacks. First and most important of all, the method has a high computational cost. Since the space of possible parameter values must be closely sampled, a high number of coherence analyses needs to be carried out. The second drawback lies in the method's sensitivity to the aperture of the local stacking operators. An adequate aperture is problem dependent and thus hard to know in advance.

In this work, we have shown that it is possible to overcome these problems by a different approach to

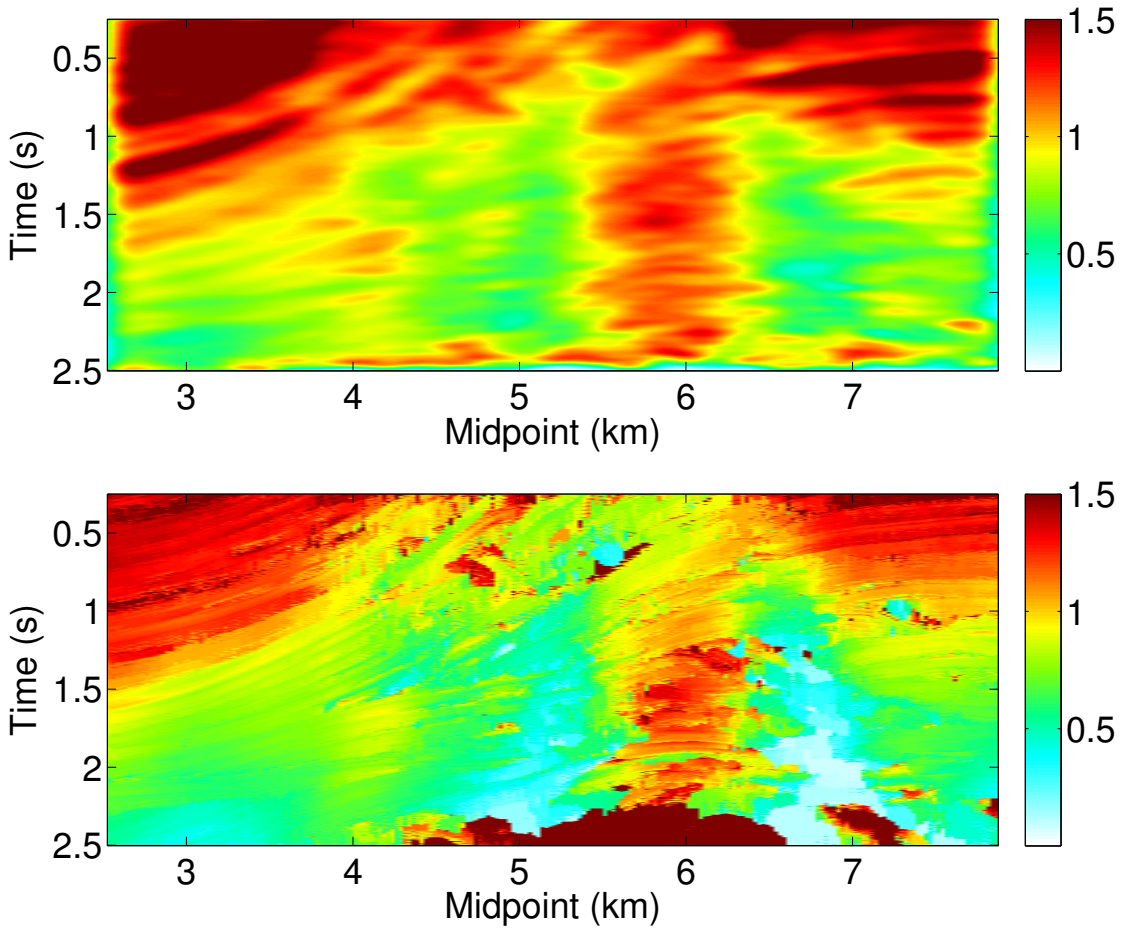


**Figure 8:** Values of CRS parameter $C$ as extracted using local slopes (top) and a simplified CRS procedure (bottom).

parameter extraction. We have presented an application of modern local-slope-extraction techniques so as to allow for the detection of the complete set of CRS parameters. The necessary information about the CRS parameters is contained in the slopes of the common-midpoint section at and common-offset sections around the central point. We have compared two techniques of extracting the CRS parameters from these local slopes. As demonstrated by a synthetic data example, the slope extraction is sufficiently robust to allow for high-quality extraction of all CRS parameters from the extracted slope fields. In this way, the CRS parameter extraction can be sped up by several orders of magnitude. It is to be expected that the improvement is even larger in 3D CRS, where eight instead of three parameters need to be determined.

Our most realistic data example using the Marmousoft data set indicates that conventionally extracted CRS parameters are superior to those obtained from local slopes. This suggests to use the slope-extracted parameters as initial values for a subsequent global search. Since conventional CRS processing uses single-parameter optimizations in data subsets to determine these initial values, such a procedure will still imply a reduced overall processing time.

## ACKNOWLEDGMENTS

This work was kindly supported by the Brazilian research agencies CAPES, FINEP, and CNPq, as well as Petrobras and the sponsors of the *Wave Inversion Technology (WIT) Consortium*.

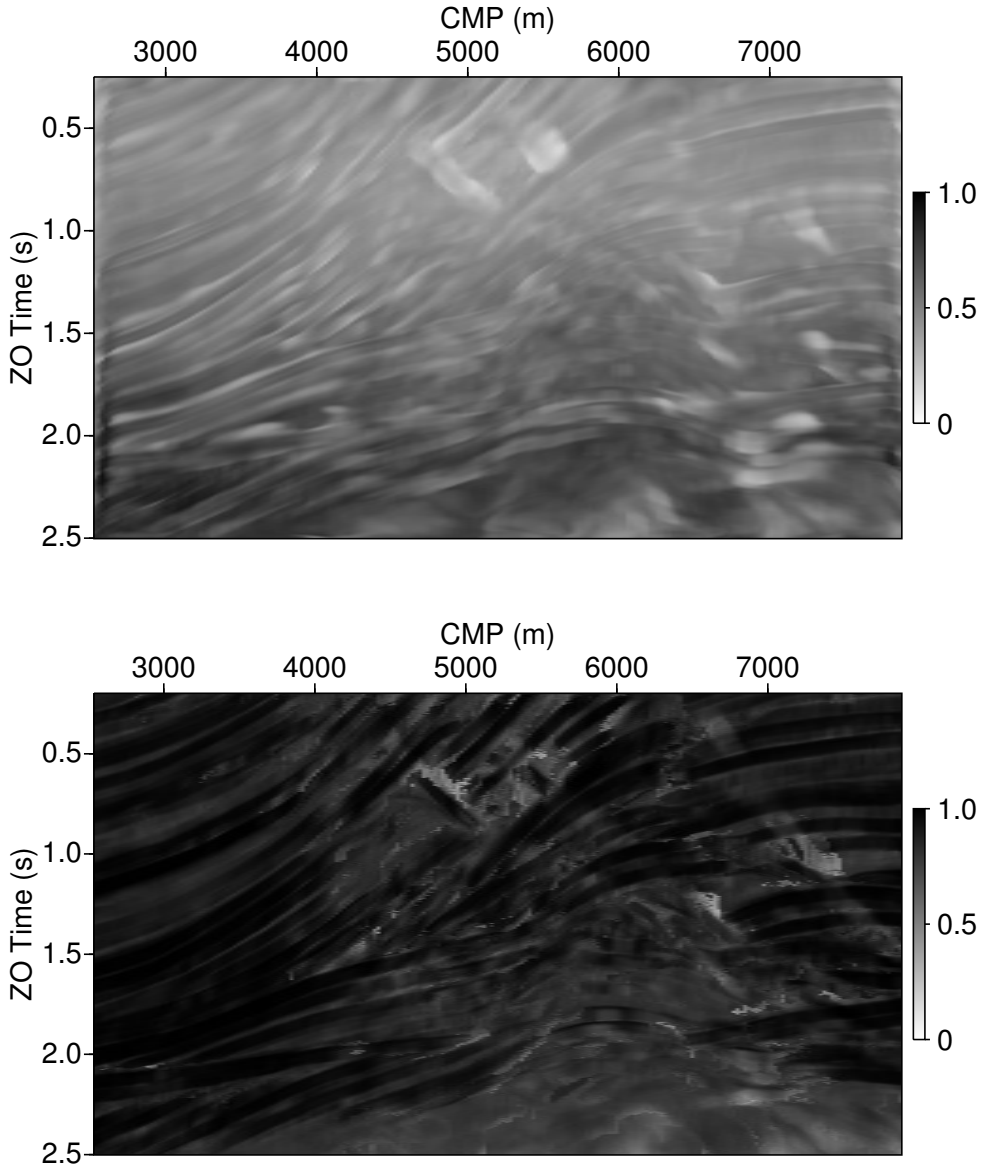


**Figure 9:** Semblance sections using the values of the CRS parameters as extracted using local slopes (top) and a simplified CRS procedure (bottom).

## REFERENCES

Billette, F. and Lambaré, G. (1998). Velocity macro-model estimation from seismic reflection data by stereotomography. *Geophys. J. Int.*, 135(2):671–690.

Billette, F., Le Bégat, S., Podvin, P., and Lambaré, G. (2003). Practical aspects and applications of 2D stereotomography. *Geophysics*, 68(3):1008–1021.

Biondi, B. (1990). *Seismic velocity estimation by beam stack*. PhD thesis, Stanford University.

Castagna, J. P. and Backus, M. M. (1993). *Offset-Dependent Reflectivity – Theory and Practice of AVO Analysis*. SEG.

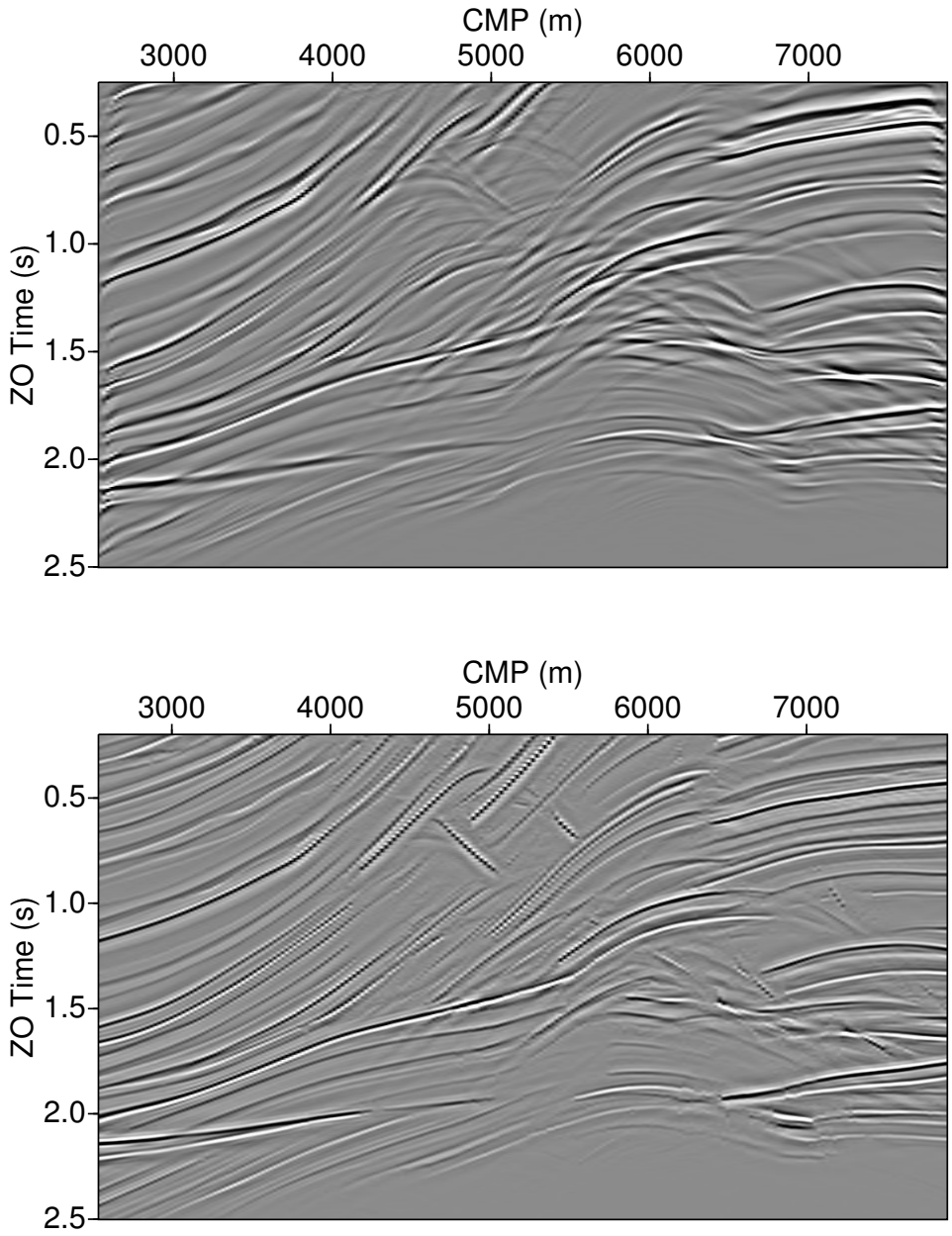


**Figure 10:** Stacked sections using the values of the CRS parameters as extracted using local slopes (top) and a simplified CRS procedure (bottom).

Claerbout, J. F. (1992). *Earth Sounding Analysis: Processing versus Inversion*. Blackwell Scientific Publications.

Duveneck, E. (2004). 3D tomographic velocity model estimation with kinematic wavefield attributes. *Geophysical Prospecting*, 52:535–545.

Fomel, S. (2002). Applications of plane-wave destruction filters. *Geophysics*, 67:1946–1960.

Fomel, S. (2007a). Shaping regularization in geophysical-estimation problems. *Geophysics*, 72:R29–R36.

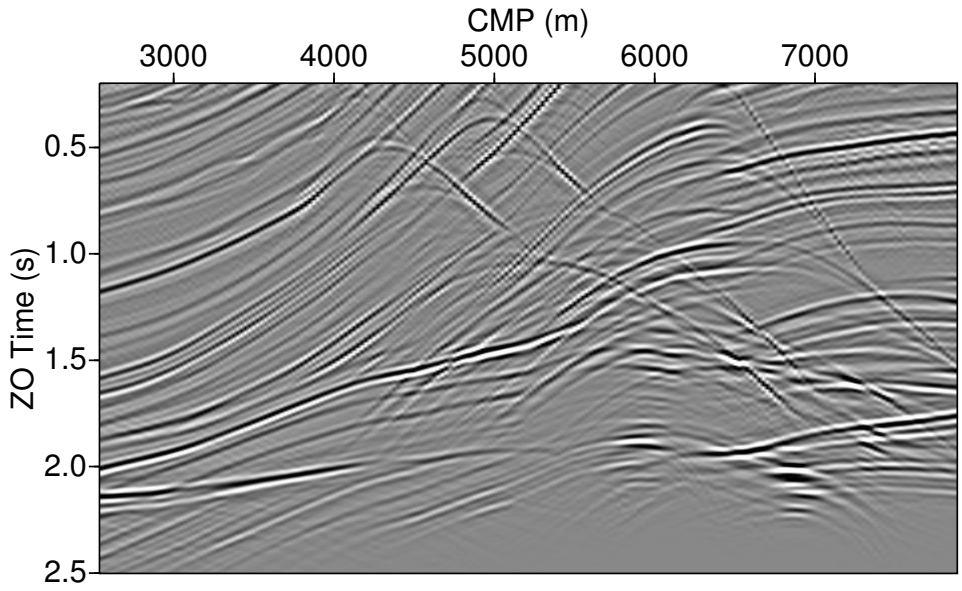


**Figure 11:** Nearest offset (100 m) of the Marmousoft data.

Fomel, S. (2007b). Velocity-independent time-domain seismic imaging using local event slopes. *Geophysics*, 72:S139–S147.

Gelchinsky, B. (1988). The common reflecting element (CRE) method (non-uniform asymmetric multifold system). *Exploration Geophysics*, 19(2):71–75.

Gelchinsky, B. (1989). Homeomorphic imaging in processing and interpretation of seismic data (fundamentals and schemes). *SEG, Expanded Abstracts*, 8(1):983–988.

Hertweck, T., Schleicher, J., and Mann, J. (2007). Data stacking beyond CMP. *The Leading Edge*, 26(7):818–827.

Hubral, P. (1983). Computing true amplitude reflections in a laterally inhomogeneous earth. *Geophysics*, 48:1051–1062.

Hubral, P., Höcht, G., and Jäger, R. (1998a). An introduction to the common reflection surface stack. In *60th Conference & Exhibition, Europ. Assoc. Geosci. Eng.* Session 1-19.

Hubral, P., Höcht, G., and Jäger, R. (1998b). An introduction to the common reflection surface stack. *60th EAGE Conference & Exhibition, Expanded Abstracts*, Session:01–19.

Jäger, R., Mann, J., Höcht, G., and Hubral, P. (2001). Common-reflection-surface stack: Image and attributes. *Geophysics*, 66(1):97–109.

Kazinnik, R. and Burnett, W. (2010). Multifold parameters by predicitive painting without scanning. *SEG, Expanded Abstracts*, pages 3639–3644.

Landa, E., Gurevich, B., Keydar, S., and Trachtman, P. (1999). Application of multifocusing method for subsurface imaging. *Journal of Applied Geophysics*, 42(3-4):283–300.

Müller, T. (1998). Common Reflection Surface Stack versus NMO/Stack and NMO/DMO/Stack. In *60th Conference & Exhibition, Europ. Assoc. Geosci. Eng.* Session 1-20.

Ottolini, R. (1983a). Signal/noise separation in dip space. *SEP report*, SEP-37:143–149.

Ottolini, R. (1983b). Velocity independent seismic imaging. *SEP report*, SEP-37:59–67.

Santos, L. T. and Schleicher, J. (2009). Improving the fast estimation of CRS parameters using local slopes. *Annual WIT Report*, 13:258–269.

Santos, L. T. and Schleicher, J. (2010). Improving the fast estimation of CRS parameters using local slopes. *SEG, Expanded Abstracts*, 29(1):3619–3623.

Santos, L. T., Schleicher, J., Costa, J. C., and Novais, A. (2008). Fast estimation of CRS parameters using local slopes. *Annual WIT Report*, 12:219–229.

Santos, L. T., Schleicher, J., Costa, J. C., and Novais, A. (2009). Fast estimation of CRS parameters using local slopes. *SEG, Expanded Abstracts*, 28(1):3735–3739.

Schleicher, J., Costa, J. C., Santos, L. T., Novais, A., and Tygel, M. (2009). On the estimation of local slopes. *Geophysics*, 74:P25–P33.

Sword, C. H. (1987). *Tomographic determination of interval velocities from reflection seismic data: The method of controlled directional reception*. PhD thesis, Stanford University.

Wolf, K., Rosales, D., Guitton, A., and Claerbout, J. (2004). Robust moveout without velocity picking. *SEG, Expanded Abstracts*, 23(1):2423–2426.